atmosphere

MDPI

Article

Asian Long-Range Transport in Relation to Atmospheric Rivers in Northern California

Catherine N. Liu [1], Sen Chiao [1,*] and Ju-Mee Ryoo [2]

[1] Center for Applied Atmospheric Research and Education, San José State University, San José, CA 95192, USA; catherine.n.liu@sjsu.edu
[2] NASA Ames Research Center, Mountain View, CA 94035, USA; ju-mee.ryoo@nasa.gov
* Correspondence: sen.chiao@sjsu.edu; Tel.: +1-408-924-5204

Received: 30 April 2019; Accepted: 31 May 2019; Published: 5 June 2019

Abstract: The study investigates the effect of aerosol long-range transport on precipitation over Northern California during atmospheric river (AR) events in the 2017 cold season (January–April). ARs in 2017 were one of the strongest to date, and the intense precipitation associated with the ARs resulted in flooding, destruction of property, and contamination of water supplies. The Aerosol Optical Depth (AOD) from Moderate Resolution Imaging Spectroradiometer (MODIS) data shows Asian dust traveling across the Northern Pacific Ocean along with AR events. Aerosol measurements in California, provided by the Interagency Monitoring of Protected Visual Environments (IMPROVE), show that more Asian dust tends to be observed over the coast, while non-Asian/localized dust is observed inland. A mixture of Asian and localized dust is observed over the mountains, although higher amounts of both are observed in the spring (March–April). Back trajectory analysis confirms that Asian aerosols are transported along the air parcels, and each AR event has its own transport pattern in terms of horizontal advection and vertical lifting. Correlation between precipitation and aerosols is low. This suggests that aerosols contribute little to the decrease of local precipitation during the 2017 AR events.

Keywords: atmospheric rivers; Asian long-range transport; aerosols

1. Introduction

In April 2017, California lifted its State of Emergency that had been declared in January 2014 in response to a five-year drought [1]. The 2017 water year alone (October 2016–April 2017) saw significant amounts of rain, with the majority of station readings in California reading above 130% of normal levels. For example, Los Angeles International Airport reached 133% of its normal rain total, compared to the previous year at 55% of its normal level [2]. While the rain alleviated drought conditions within the state, the intense precipitation resulted in a flooding of cities and freeways, mudslides and mountain trail erosions, destruction of property, and contamination of water supplies; all of which threaten public safety.

The motivation for the study is to improve precipitation forecasts and prepare for future extreme events by understanding the dynamics and characteristics of atmospheric phenomena that contribute to US west coast precipitation amounts. To start, most of California's rainfall arrives during the cool months (October–March), when low level jets draw heat and moisture from the tropics, near Hawaii, northeastward to the midlatitudes [3]. This strip of heat and moisture to the North American West Coast is commonly known as the Pineapple Express, or an Atmospheric River (AR) [4]. ARs are usually characterized by a length of around 2000 km and a width up to 1000 km. The air column typically has at least 2 cm of integrated water vapor (IWV), or greater than 250 kg m^{-1} s^{-1} of integrated water vapor transport (IVT), within the first 2.5 km from the surface, and a center of strong winds at 2 km [5,6].

Recent studies have been using IVT measurements in place of IWV, since IVT is highly correlated with winter precipitation over the U.S. West Coast [7], as well as its strong correlation with precipitation over terrain [3,5,8]. The 2017 heavy rainfall events, attributed to consecutive AR events that occurred multiple times during January and February, gives rise to the question: What made the 2017 AR events occur more frequently, and with more rainfall? One consideration is cloud-aerosol interactions, particularly due to long-range transport. Long-range transport is used to describe aerosol and gas transfer through the atmosphere between continents, which has the potential to increase greenhouse gas (GHG) concentrations, such as surface ozone, and particulate matter in other parts of the globe outside their place of origin [8]. For example, Ding et al. (2013) used Lagrangian particle dispersion modeling (LPDM) with the Hybrid Single-Particle Lagrangian Integrated Trajectory model (HYSPLIT), and found that the increase in ozone and carbon monoxide had traveled to Hong Kong from Southeast China via long-range transport [9]. Although the distance traveled is not as far as the Northern Pacific Ocean, the study showed how aerosol transport affects locations outside of their original locations. More importantly, the aerosols affect the microphysics in clouds by acting as cloud condensation nuclei (CCN) and ice nuclei (IN) [10]. As a result, public health and local environmental conditions are affected [8].

Previous studies indicate that Asia is the leading contributor of anthropogenic aerosols over the North Pacific, and that North America, which is situated downwind, receives much of that pollution [8,11]. With an increase of particulate matter in the atmosphere, there is an interest in Asian aerosol effects on cloud dynamics, such as deep convective clouds over the North Pacific Ocean [12,13]. Aerosol long-range transport from the Asian continent to the West Coast of the United States consists of two pathways, referred to as the outflow (from the Asian continent) and import (to the North American continent) [11]. First, as convection occurs, aerosols are injected upwards into the troposphere where they are transported across the Northern Pacific via midlatitude cyclones, and this is especially strong in the spring and summer. As aerosols reach the Northeastern Pacific, those in the free troposphere are pulled westerly through advection, while those closer to the surface are transported directly along the boundary layer. The free troposphere transport then continues with either subsidence in the subtropical Pacific high, or through dry air in the upper troposphere sinking behind cold fronts, or by subsidence induced by mountain waves as it crosses the North American Western Coast [11].

One of the uncertainties that contribute to the difficulty in understanding cloud dynamics is the effects of aerosols on cloud microphysics. As mentioned earlier, aerosols function as CCN and IN, the building blocks of cloud formation. Uncertainties result from aerosol properties, e.g., mineral versus anthropogenic, which have varied effects upon cloud growth, and precipitation location and intensity. In some cases, studies have shown different findings for the same aerosols [10,14–17]. Creamean et al. (2013) found that dust aerosols, originating from a number of deserts, ranging from the Sahara in Africa to the Gobi and Taklimakan in Asia, were a key factor for the IN formation, invigorated convection, and enhanced precipitation, especially in mixed-phase clouds [10]. Also, aerosols lifted to heights of at least 5000 m were able to travel longer distances, as seen with the Taklimakan desert dust that was recorded to have circled the earth in thirteen days. Their study also discussed the seasonality of dust aerosol with Taklimakan dust detection maximums between April and May. The Gobi Desert, despite being frozen during the winter, is still an important dust source because of the strong Siberian winter storms that blow through it. Lastly, the Sahara is a major mineral source, since dust is lifted all year round, and not limited seasonally like the Taklimakan or Gobi deserts. Ault et al. (2011) also showed that dust leads to the formation of IN, increasing riming rates, the rate at which frost covers an ice particle, and increasing the precipitation efficiency [16]. While Creamean et al. (2013) [10] and Ault et al. (2011) [16] showed IN formation due to dust, which contributes to an increase in precipitation, Patil et al. (2017) [17], on the other hand, found in their study that an increase in Asian dust aerosols inhibited deep convective clouds and ice water paths, leading to an increase in cloud top pressure, almost opposite of what was recorded by the other two studies.

Despite the discrepancies in dust aerosol effects in various studies, they all agree that aerosol transport is the strongest in the spring, when Asian dust and pollution emissions are the highest [8,10,16–18]. However, little to no literature has described the extent and effects of Asian aerosol transport on the US West Coast during the cool months (October–March) in terms of atmospheric processes (precipitation, development, etc.). That being said, Ault et al. (2011) [16] detected mineral dust from Asia in orographic precipitation over California during the CalWater Early Start campaign, which examined two extratropical cyclone systems between 22 February and 11 March 2009. The enhancement of horizontal IVT and IWV concentrations that resulted from the two systems were attributed to AR conditions.

Still, the question of how the long-range transport of Asian aerosols affect precipitation amounts, system location, and AR frequency, particularly for the 2017 events, remains. The study will compare the properties of six 2017 AR events to a ten year (2006–2016) climatology, in order to (1) understand the effect of Asian long-range aerosol transport on different locations over Northern California during ARs, (2) examine how the long-range transport of aerosols affect precipitation intensity, location, and the frequency of ARs over Northern California, and (3) assess how aerosols are correlated with precipitation associated with AR events. It is hypothesized that there is a positive correlation between aerosols and precipitation, in that aerosols will have contributed to the precipitation enhancement of the 2017 AR events.

2. AR Events and Synoptic Conditions in 2017

For the study, the months of January to April were taken into consideration, with a focus on the months of January and February, as the rainfall was particularly heavy during this time. The highest amounts of observed rainfall occurred at the coasts and mountains, as seen in Figure 1a [19], with amounts exceeding 20 inches (508 mm). Inland measurements were up to 6–10″ (152–254 mm). Rainfall amounts were higher overall in northern California, and decreased towards the south as well as further inland on the other side of the Sierras. This trend is also observed during the March and April months. In comparison to climatological rainfall norms collected by NOAA since 2005, the majority of California experienced a 110% to 600+% increase during January and February 2017 (Figure 1b), with the highest percentage changes in the mountains. For March and April 2017, rainfall was at or slightly below normal amounts for central California, while southern California amounts were below 50%. Most of the damages, as a result of flooding and erosion, occurred during January and February. Overall, California experienced at least 150% of its normal rainfall amounts for 2017. For this reason, case studies were taken from these two months.

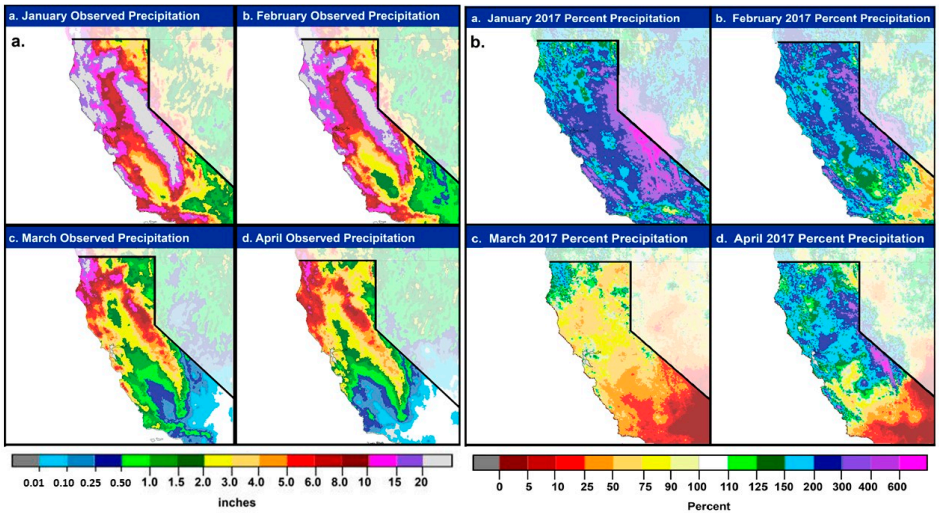

Figure 1. (**a**) Monthly observed precipitation, and (**b**) Monthly percent of normal precipitation. (Source: National Weather Service: Advanced Hydrologic Prediction Service Precipitation Analysis [19]).

2.1. January 2017

The first series of AR events occurred from 01/07–11, bringing as much as 20″ (508 mm) of rainfall to areas such as Strawberry Valley, located at the western base of the Sierras. On 01/08, the Uvas Creek in Santa Clara County flooded roads and properties up to three feet (914.40 mm), due to the Uvas Reservoir overflowing and spilling into the creek. The reservoir typically receives a monthly average of 4.88″ (124.95 mm) of rainfall during January, but experienced a max 48 h rainfall total of 7.05″ (179.07 mm) in 2017. Other incidents that occurred during this event were road flooding in Morgan Hill, and 48 h rain gauge amounts of 8.74″ (222 mm) at the Guadalupe Watershed, 9.49″ (241.05 mm) at Uvas Canyon County Park, and 6.73″ (170.94 mm) at the Lexington Reservoir. January rainfall amounts at these areas are generally 3.47″, 3.63″, and 3.97″, (88.14 mm, 92.02 mm, 100.84 mm) respectively.

The second series of AR events occurred between 01/17 and 01/19 where southern California received up to 1.5″ (38 mm) of rainfall, central California received up to 4″ (101 mm), and northern California received up to 6″ (152 mm) [20,21].

2.2. February 2017

The third series of AR events occurred between 02/06 and 02/10. Around 6.5″ (165.1 mm) were recorded for areas at higher elevations, as well as reports of river flooding in parts of Sonoma County and the San Francisco Bay area, such as the San Francisquito Creek flooding nearby businesses as well as the US highway 101 bridge. In addition, the Oroville Dam flooding incident [22] that led to the evacuation of over 188,000 people mid-February was partly caused by the heavy rainfall which the lake experienced on 02/07. The fourth series of AR events occurred between 02/15 and 02/21. From the 02/15-17, two storm systems saturated the soil, which easily led to runoff and reservoir overflow during following events, as seen with the Anderson Reservoir spillage on 02/18. On 02/21, the combination of Coyote Creek and Anderson Reservoir overflow caused numerous flooding events in San Jose, inundating several neighborhoods, businesses, and roads [20].

In terms of post flood damages, Santa Clara Valley Water District's 2017 Flooding Report estimated that San Jose identified about $50 million in private property damages, and $23 million in public property damages. Around 14,000 people were evacuated during these events, with no reports of injury or death during rescue operations [20].

2.3. Synoptic Conditions and the Observed Characteristics of ARs

The synoptic conditions for the four different AR events are examined to see if a specific synoptic condition can provide favorable conditions for enhancing the long-range aerosol transport, and how the Potential Vorticity associated with the lower-level wind, water vapor, and sea level pressure evolves with time during the AR events.

Figure 2 shows the map of ERA-Interim Potential Vorticity (PV) at 250 hPa, specific humidity (q) overlaid by the horizontal wind at 850 hPa, temperature at 850 hPa, and sea level pressure for AR events during January–February 2017. Strong upper-level troughs with large PV were located offshore near the coast of California at this time, which implied that stratospheric air through the tropopause (PVU = 1.5 PVU is regarded as a dynamic tropopause) penetrated downward to the mid-troposphere (~500 hPa, not shown). PV intrusion mostly occurred anticyclonically (i.e., clockwise rotation) over the Pacific and the western U.S., extending toward the West Coast of the U.S (Figure 2a). On 01/19/17, however, PV penetrated the western U.S. cyclonically, mimicking cyclonic wave breakings [23], and leading to stronger sea level low pressure over the northwest of California (Figure 2a,d, second row). The filamentary, northward directing water vapor bands over the Pacific reflected the response of the lower-level water vapor field to the existence of an upper level trough in the developing mid-latitude baroclinic system during AR events (Figure 2b). For all AR events, the high and narrow water vapor band was elongated from southwest to northeast with strong southwesterlies extending toward the California coast for all AR events. As shown in Figure 2a,c, a wavy structure of temperature and its

horizontal gradient also appears to be associated with the narrow and deep penetration of elevated upstream PV. Temperature was slightly cooler inland, especially in the 01/07 AR case, but this was also dependent on the location, and extent of the sea level's low and high. There were spatial differences in high and low in sea level pressure for different ARs, but di-pole patterns of the low and high pressures persisted during all AR events (Figure 2d). These strong contrasts between the sea level high and low was shown both in the Pacific and on the West Coast of the U.S., confirming that these are prominent synoptic features of AR events. Low sea level pressure also developed over the eastern North Pacific, associated with the upper level trough for all AR events.

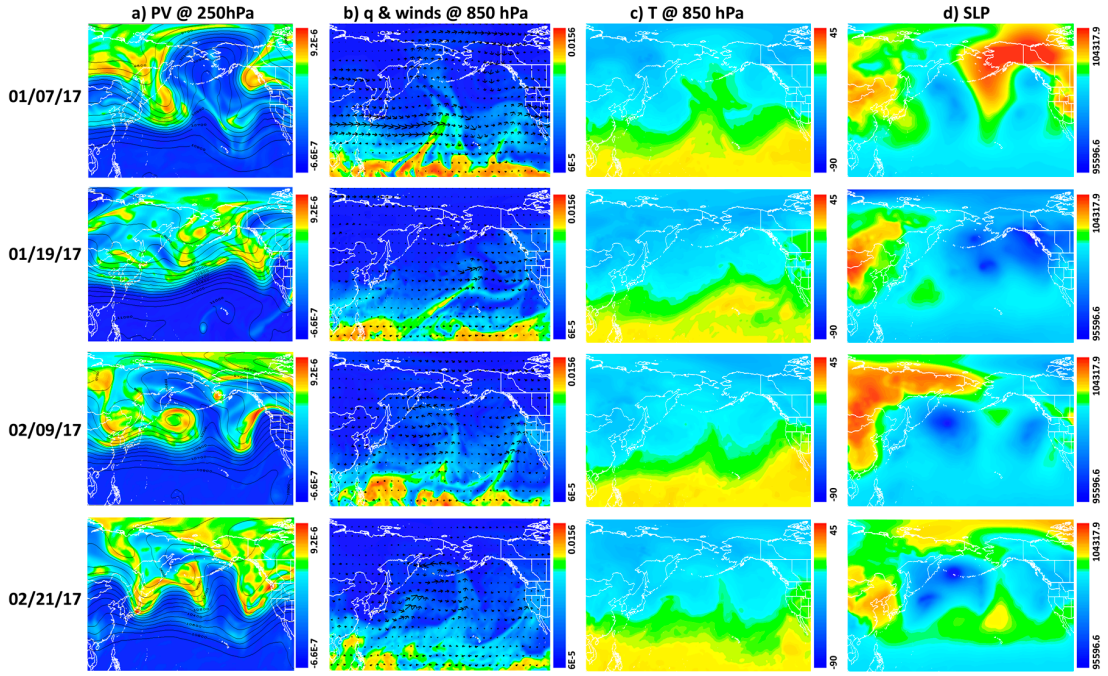

Figure 2. Longitude-latitude cross section of (**a**) potential vorticity (PV) at 250 hPa with PVU = 1.5 (1 PVU = 10^{-6} m^{-2} s^{-1} K kg^{-1}; (**b**) water vapor mixing ratio (q, g kg^{-1}) overlaid by horizontal wind vector (m s^{-1}) at 850 hPa; (**c**) temperature (in °C) at 850 hPa; (**d**) sea level pressure (Pa) at 00 UTC 01/07/17 (1st row), 01/19/17 (2nd row), 02/09/17 (3rd row), and 02/21/17 (4th row) obtained from the ERA-Interim reanalysis data.

By 2–3 days after each AR event, the higher amount of water vapor has moved inland with cooler temperature as the low pressure moved closer to the western U.S., and the upper level trough was weaker and decayed (not shown). Overall, as the AR approaches the western U.S., a strong upper-level trough with large PV penetrating either anticyclonically or cyclonically is located offshore near the coast of California, leading to strong low-level southerlies and southwesterlies over this same coast of California. This also suggests that the large-scale upper-level trough associated with upper-level jet extending toward northern California may provide a favorable condition for the long-range aerosol transport from Asia during AR events.

3. Data and Methods

3.1. Satellite Data

Moderate Resolution Imaging Spectroradiometer (MODIS) Aqua was used to note whether there was Asian long-range transport occurring during the 2017 cases chosen. Aerosol optical depth was measured daily at 500 nm with 1° resolution. MODIS data was visualized one week before the atmospheric river (AR) event, as this is the usual time it takes for Asian dust to travel across the Northern Pacific Ocean. As shown in Figure 3, there is a visible transport of aerosol across the Northern

Pacific. Cloud-cover contributes to most of the missing data, but in some cases MODIS-Aqua was able to pick up Aerosol Optical Depth (AOD) signals along the edges of cloud cover. It is acknowledged that there are limitations to using satellite data because of cloud cover. Alternate methods would be the use of Lidar to visualize from the surface up, however this is not currently possible over the ocean. In the case of CALIPSO data, the swath rarely went over the areas of interest. Another alternative would be to use reanalysis or model data, however this study's scope was to first use observational data.

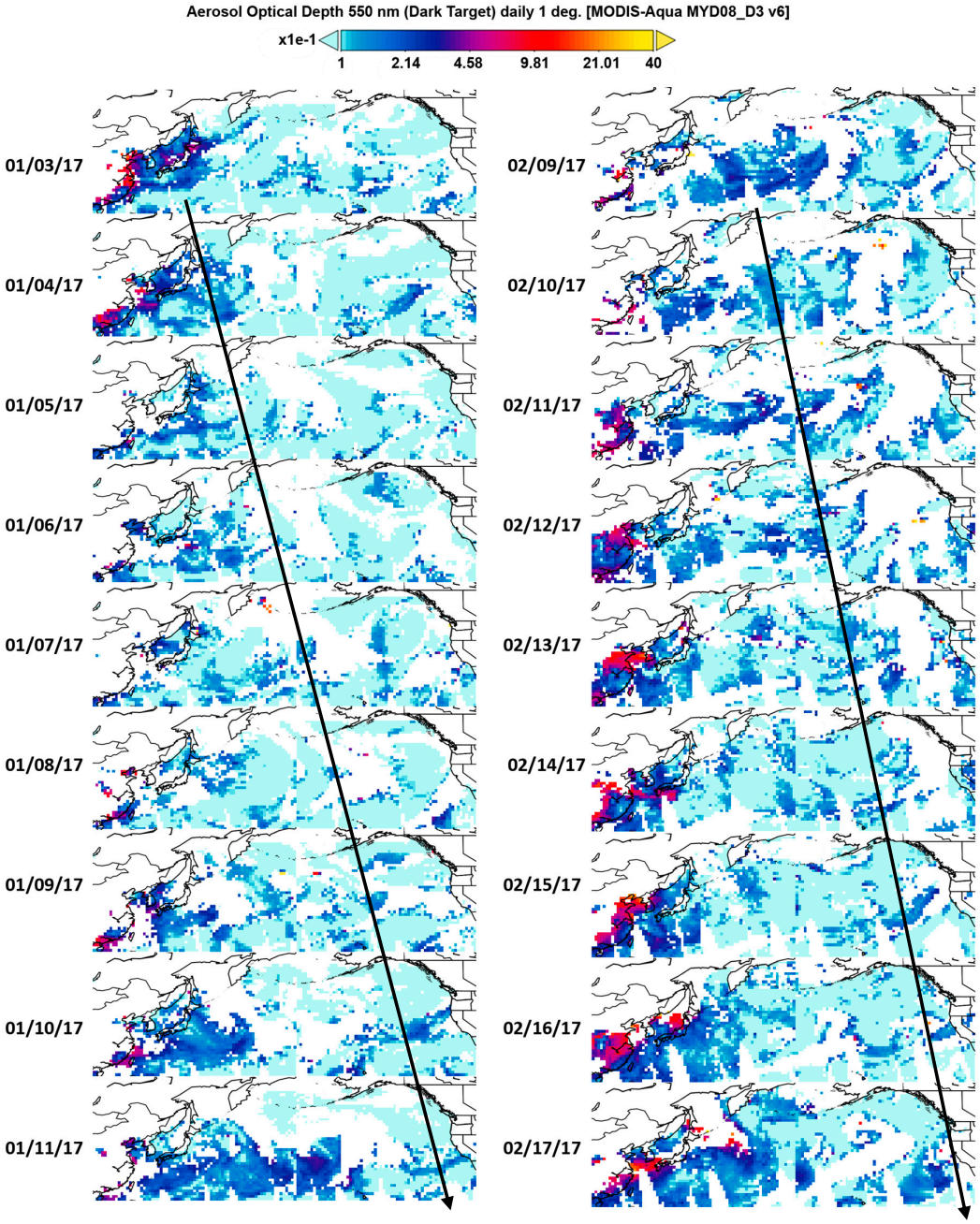

Figure 3. 2017 Daily 1° Moderate Resolution Imaging Spectroradiometer-Aqua Aerosol Optical Depth (MODIS-AOD) (550 nm) for the period of (**a**) 01/03–11, and (**b**) 02/09–17. These are examples of atmospheric river (AR) events that occurred in January and February. Satellite imaging was examined 5+ days before the 01/11 and 02/16 AR events. Black lines represent aerosol particulates being transported across the Northern Pacific during AR event weeks.

The Special Sensor Microwave Imager Sounder (SSMIS; Wentz et al. (2012) [24]) provided by NOAA/NESDIS at 0.25° grid spacing and average twice daily (e.g., 00–12Z and 12–24Z) was employed to visualize the AR event progression off the coast of the Western United States from January and February (Figure 4). Some selected examples of four case studies (01/07–10, 01/17–19, 02/06–10, 02/15–21) are shown in Figure 4. AR events can be identified when water vapor amounts to above at least 2 cm of integrated water vapor (IWV).

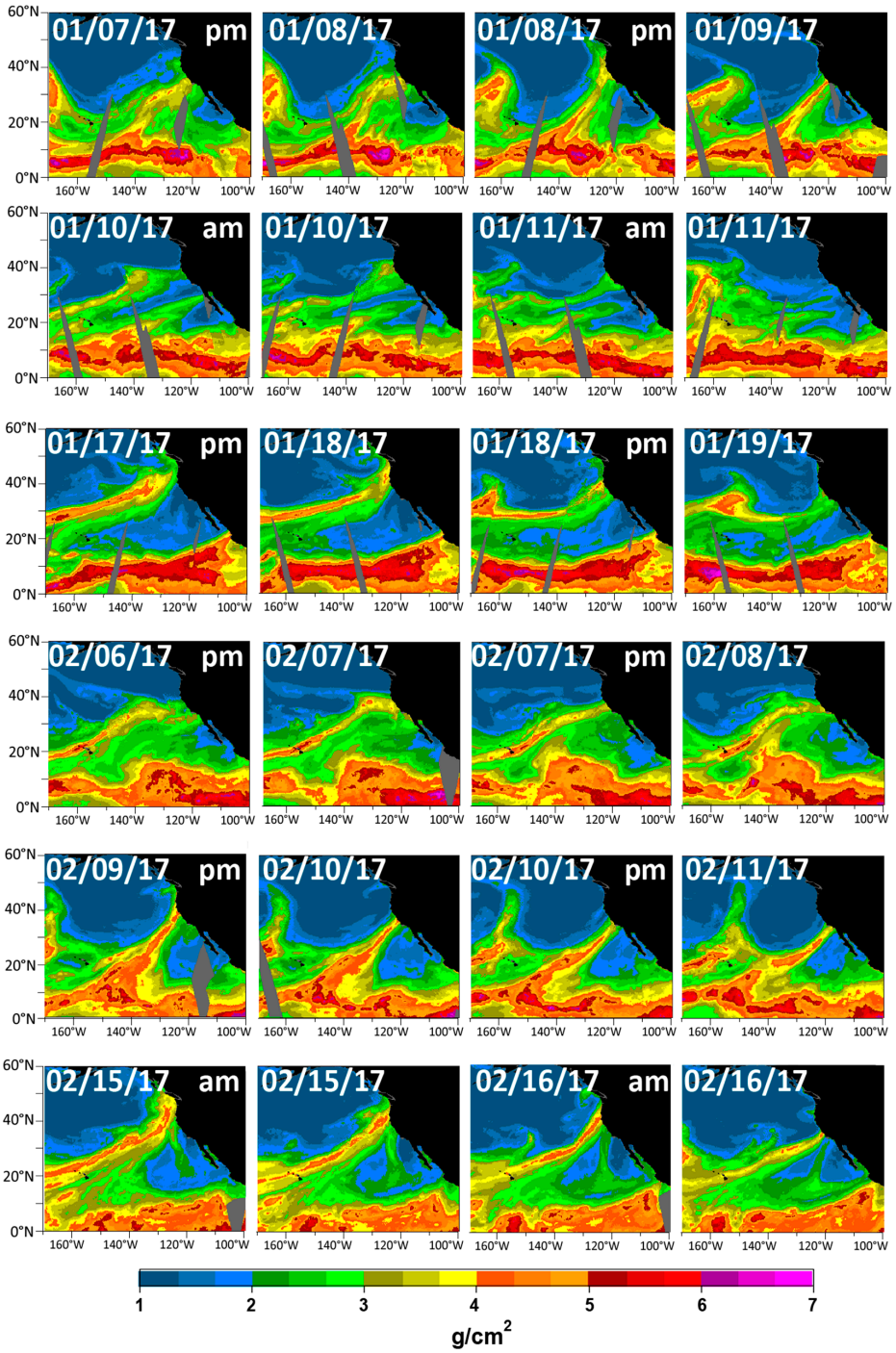

Figure 4. The Special Sensor Microwave Imager Sounder (SSMIS) integrated water vapor (IWV) 0.25° grid spacing and average twice daily from 0–12Z (AM) and 12–24Z (PM) for four AR events, 01/07–11, 01/17–19, 02/06–10, 02/15–21 of 2017. Examples of AR events that occurred during these time periods are shown. Water vapor amounts above at least 4 g/cm^2 (>2 cm [7]) represents an AR.

3.2. Observation Site Data

The Interagency Monitoring of Protected Visual Environments (IMPROVE) data was used for aerosols measurements in California [10,18,25,26]. Data measurements were taken for twenty-four hours every three days. For the study, a combination of sites were used to represent differences between coastal (Redwood National Park, Point Reyes National Shores, Pinnacles National Park), inland (Trinity, Fresno), and mountainous (Lassen Volcanic National Park, Bliss State Park, Kaiser) areas (Figure 5). The site Trinity was dropped from the final analysis since measurements from there ended in 2015. Therefore, Fresno was the only site to represent inland conditions.

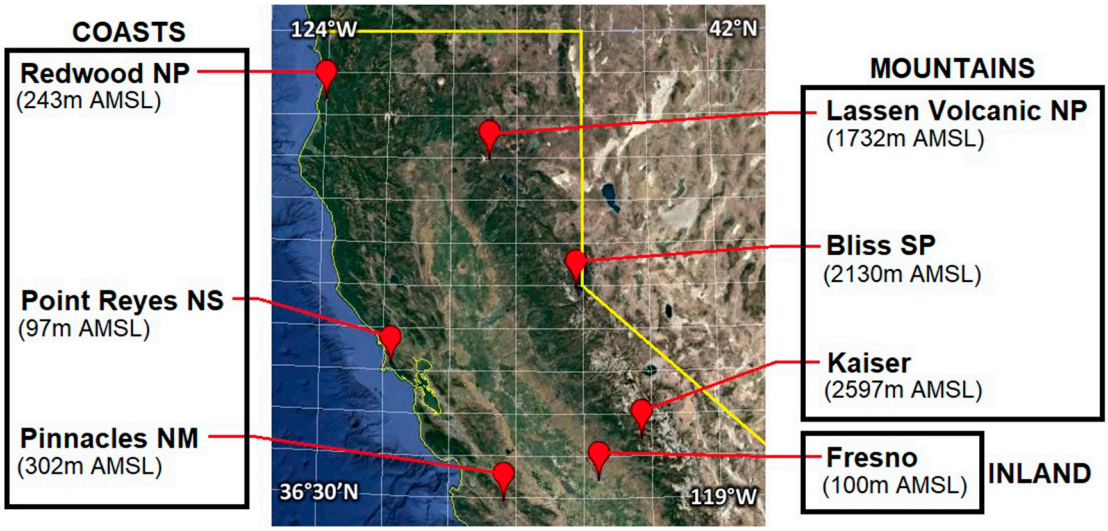

Figure 5. The seven observational sites used in the study were taken to represent data at coastal (Redwood NP, Point Reyes NS, and Pinnacles NM), inland (Fresno), and mountainous (Lassen Volcanic NP, Bliss SP, and Kaiser) regions. Elevation was recorded in units of meters above mean sea level.

Iron, calcium, and soil measurements were used to determine Asian dust amounts at the sites. Using a method employed in Creamean et al. (2014), the dust source was separated into Asian or localized, using a ratio of iron (Fe) to calcium (Ca), which is generally accepted as the composition of Asian desert dust [26,27]. Ratios less than a value of one indicated Asian dust presence, hence long-range transport, while ratios greater than one indicated localized dust. Based on Fe/Ca ratios in Equation (1), soil amounts for each site were categorized as either Asian dust or Non-Asian dust for simplicity.

$$if \begin{cases} \frac{Fe}{Ca} < 1 : Asian\ dust \\ \frac{Fe}{Ca} > 1 : Localized\ dust \end{cases} \quad (1)$$

Other aerosols analyzed from the sites were black carbon (BC) and sulfate (SO_4).

3.3. Precipitation Data

Integrated water vapor transport measurements were taken from Modern-Era Retrospective analysis for Research and Applications, version 2.1 (MERRA 2), with a horizontal resolution of 0.5° by 0.66°. 3-hourly reanalysis data was provided by the AR catalog created by Rutz et al. (2014) [7]. Due to the fact that this was a gridded dataset, the integrated water vapor transport (IVT) measurements were extracted to be the closest to the IMPROVE site locations.

To match with IMPROVE dataset dates, daily IVT averages were calculated from the 3-hourly MERRA dataset. IVT measurements were used calculate AR frequency and strength as later discussed in Section 4.2. The Climate Prediction Center Unified Gauge-Based Analysis of Daily Precipitation over CONUS Real-time was used for daily precipitation measurements. The dataset has a resolution of 0.25° × 0.25°, and was manipulated to match IMPROVE's every 3-day temporal resolution.

3.4. Back Trajectory Model Simulation

The NOAA Hybrid Single-Particle Lagrangian Integrated Trajectory model (HYSPLIT) model was used to analyze parcel back trajectories [26]. The Global Data Assimilation System (GDAS) 0.5 degree archive ensembles at Redwood NP (coast), Fresno (inland), and Lassen Volcanic NP (mountain) were simulated at 3, 5, and 7 km for 10 days. These three heights were chosen to observe parcel lifting during the track. During model set-up, heights were chosen in meters, but are displayed in hPa for the trajectory plots. This was to provide an easier way of following parcel heights along the track as well as comparison with synoptic plots.

4. Results

4.1. Dust Measurements

The total dust amounts from 01/01 to 04/28 from the seven sites are investigated. As shown in Figure 6, there is an increase in instances of localized dust presence as the system moves southward among the coastal sites. In terms of the inland site, Fresno dust measurements are mainly attributed to localized dust, which is most likely the result of its surrounding city and/or agricultural land. At the mountainous sites, elevation differences might be a reason for why the mountainous sites did not follow the North-South decrease in Asian dust trends. For example, site measurements could be influenced by whether the site was located toward or away from the windward direction, or influenced by localized terrain differences. Overall, these results are similar to findings in Rutz et al. (2014) [7].

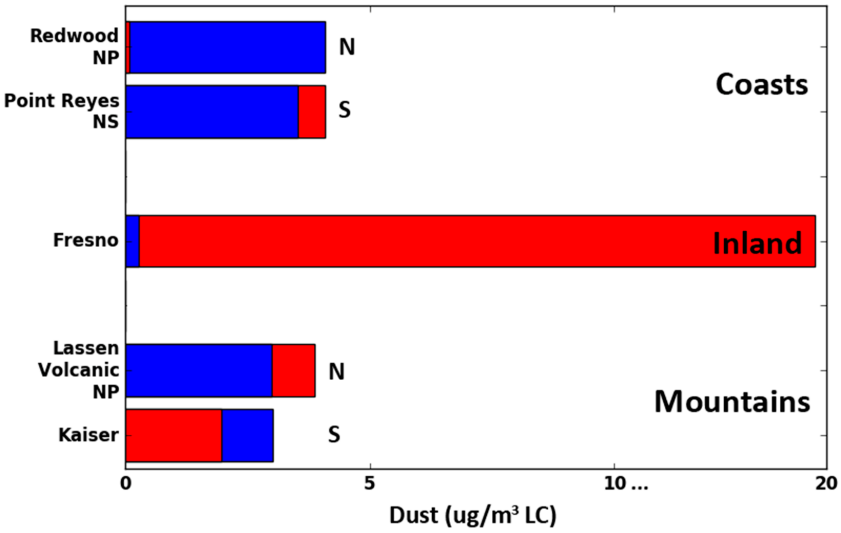

Figure 6. 2017 Total dust amounts. The most northern and southern site for the coastal and mountainous regions were selected to show aerosol patterns as the AR system moves along the US West Coast. At each site, dust amounts are totaled from January to April, then separated into Asian-influenced (blue) or non-Asian/localized dust influenced (red).

4.2. 2006–2016 Climatological Analysis in Comparison to 2017

The evolution of aerosol for January–April from 2006 to 2016 were constructed. Redwood NP, Fresno, and Lassen Volcanic NP are shown to represent coasts, inlands, and mountains, respectively, (Figure 7). It is seen that the majority of dust amounts at coastal sites are attributed to Asia, with some amounts being due to localized dust. Inland at Fresno, localized dust is in the majority with hardly any trace of Asian influenced dust. Again, this is not surprising considering Fresno is located in the valley, where it is expected that localized dust is trapped compared to coastal or mountainous sites. Lastly, the majority of Asian and locally influenced dust varies from year to year at the mountainous regions.

This is more so in the case of Lassen Volcanic NP, due the fact that the observation site is located at a lower elevation on the windward side of the mountain.

AR frequency and strength comparisons between the 2006 and 2016 climatology and year 2017 were conducted (Table 1). For example, Redwood NP usually receives around 4 AR events per year. This was calculated by visually counting the number of IVT peaks greater than 250 kg m^{-1} s^{-1} (not shown). 2017 experienced 5 AR events, one moderate event and four weak events, according to the strength chart created by Ralph et al. This chart categorizes AR strength by IVT measurements, where 250–500 kg m^{-1} s^{-1} are weak events, 500–750 kg m^{-1} s^{-1} are moderate events, 750–1000 kg m^{-1} s^{-1} are strong events, 1000–1250 kg m^{-1} s^{-1} are extreme events, and greater than 1250 kg m^{-1} s^{-1} are exceptional events. Besides 2017, the years 2010, 2012, 2014 and 2015 also experienced moderate AR events. 2012 experienced five weak and one moderate AR event, while 2010 and 2015 experienced 2 weak and one moderate AR event. Point Reyes NS, further south, typically receives an average of 5 weak AR events. However, 2017 experienced 11 weak events. Likewise at Pinnacles NP, 2017 experienced 6 weak events, when the site typically receives 1–2 AR events. Inland at Fresno, similar to results found above, the site receives 1–2 events climatologically, while three occurred in 2017. Similarly at the mountainous sites, from north to south, Lassen Volcanic NP, Bliss SP, and Kaiser received six, five, and four weak events, respectively, in 2017. From 2006 to 2016, the sites usually received an average of 3, 1, and no AR events, respectively. Table 1 summarizes 2006–2017AR frequencies and strengths. For each site, AR frequency and strength were determined based on (1) the number IVT peaks above 250 kg m^{-1} s^{-1} for a given year, which is the minimum IVT level for an AR event to be present, and (2) classifying strength based on the chart created by Ralph et al. (2019) [28]: Weak (250–500 kg m^{-1} s^{-1}), moderate (500–750 kg m^{-1} s^{-1}), strong (750–1000 kg m^{-1} s^{-1}), extreme (1000–1250 kg m^{-1} s^{-1}), and exceptional (>1250 kg m^{-1} s^{-1}). Overall, 2017 has seen more frequent AR events compared to the last 10 years.

Table 1. January–April 2006–2017 AR Frequency and Strength. For each site and year (Y), AR frequency (frq) and strength (str) were determined based on (1) the number integrated water vapor transport (IVT) peaks above 250 kg m^{-1} s^{-1} for a given year as seen in Figure 7, which is the minimum IVT level for an AR event to be present, and (2) classifying strength based on the chart created by Ralph et al. (2019) [28]: Weak (250–500 m^{-1} s^{-1}), moderate (500–750 m^{-1} s^{-1}), strong (750–1000 m^{-1} s^{-1}), extreme (1000–1250 m^{-1} s^{-1}), and exceptional (>1250 m^{-1} s^{-1}). Redwood NP: rdwd; Point Reyes NS: ptrey; Pinnacles NM: pinn; Fresno: fres; Lassen Volcanic: NP lavo; Bliss SP: bliss; and Kaiser: kais.

Coasts									Inland			Mountains								
rdwd			ptrey			pinn			fres			lavo			bliss			kais		
Y	frq	str	Y	frq	str	Y	frq	str	Y	frq	str	Y	frq	str	Y	frq	str	Y	frq	str
6	5	w	**6**	6 1	wm	**6**	1 1	wm	**6**	1 1	wm	**6**	3	w	**6**	0	—	**6**	0	—
7	1	w	**7**	3	w	**7**	2	w	**7**	0	—	**7**	0	—	**7**	0	—	**7**	0	—
8	1	w	**8**	2	w	**8**	1	w	**8**	1	—	**8**	0	—	**8**	1	w	**8**	0	—
9	4	w	**9**	3 1	wm	**9**	3	w	**9**	0	—	**9**	3	w	**9**	1	w	**9**	0	—
10	3 1	wm	**10**	5	w	**10**	1	w	**10**	1	w	**10**	3	w	**10**	1	w	**10**	0	—
11	4	w	**11**	8	w	**11**	3	w	**11**	2	w	**11**	3	w	**11**	1	w	**11**	0	—
12	5 1	wm	**12**	7	w	**12**	1	w	**12**	2	w	**12**	3	w	**12**	0	—	**12**	0	—
13	1	w	**13**	0	w	**13**	1	w	**13**	0	—	**13**	0	—	**13**	0	—	**13**	0	—
14	1 1	wm	**14**	6	w	**14**	2	w	**14**	3	w	**14**	3	w	**14**	0	—	**14**	0	—
15	3 1	wm	**15**	2	w	**15**	2	w	**15**	0	—	**15**	2	w	**15**	0	—	**15**	0	—
16	4	w	**16**	8	w	**16**	2	w	**16**	1	w	**16**	2	w	**16**	0	—	**16**	0	—
17	4 1	wm	**17**	11	w	**17**	6	w	**17**	3	w	**17**	6	w	**17**	5	w	**17**	4	w

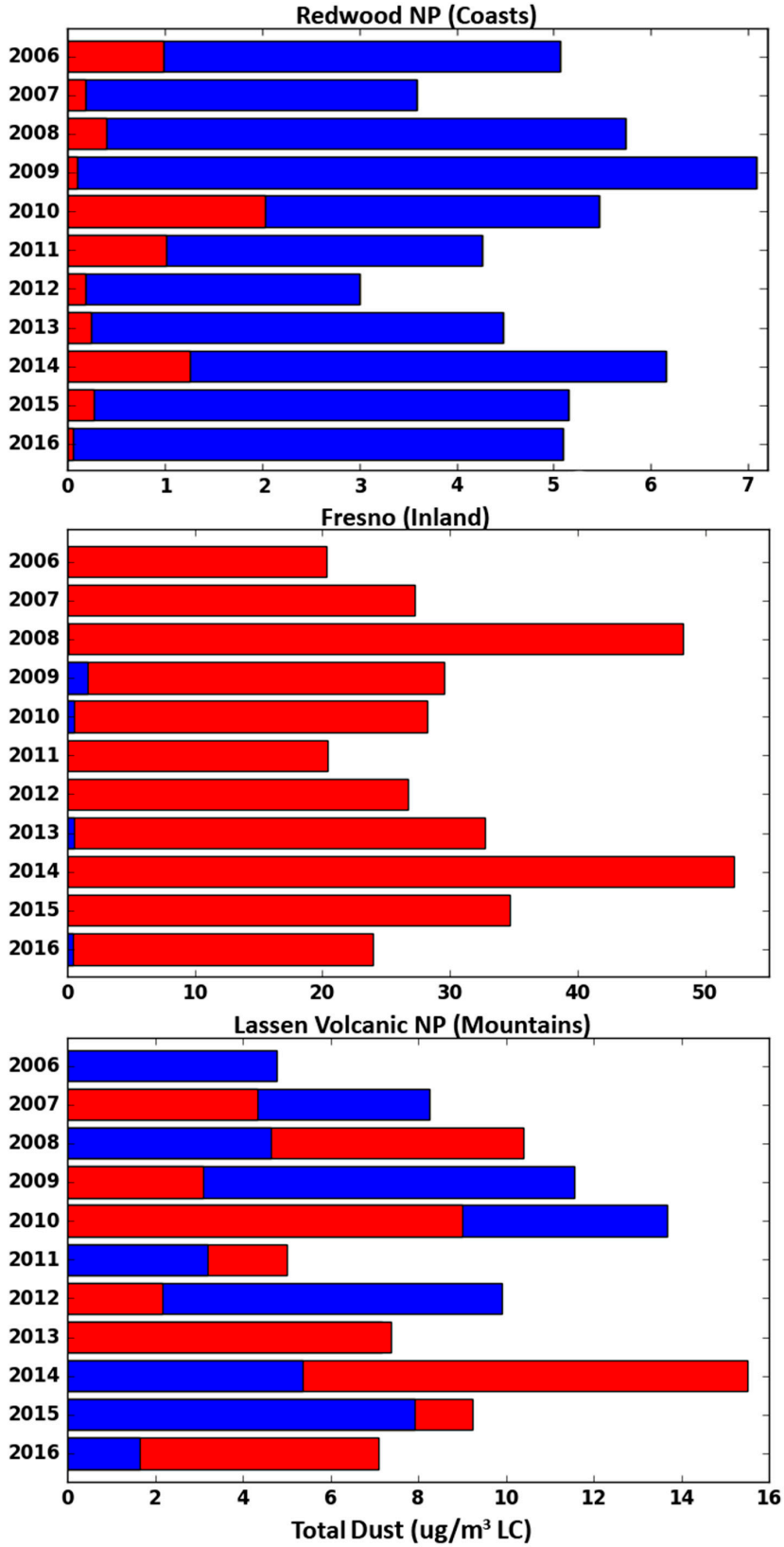

Figure 7. 2006–2016 aerosols. Dust amounts per year were totaled then separated to examine how much of that dust was Asian and non-Asian influenced.

In addition to dust, black carbon (BC) and sulfate (SO_4) were also measured at each site. A correlation analysis was conducted between these three aerosol types and precipitation amounts.

Figure 8 shows the correlation at coasts, inlands and mountains sites from climatological data (2007–2016) compared to 2017. NCEP CPC RT data begins in 2017, therefore climatological correlations were calculated from 2007 to 2016. Table 2 summarizes the correlation coefficient (R-values) for all sites. Overall, R-values vary from being low climatologically, and in the 0.30–40 s for 2017 data. Correlation values with low *p*-values ($\alpha = 0.10$) of 0.10 or less are statistically significant and are highlighted. Most of the correlations for both time periods are negative, meaning that aerosols were found to have a suppressing effect on precipitation. This trend was also found when calculating correlations between aerosols and IVT (not shown). Starting with climatological data, statistically significant correlation values appear to be Asian dust and SO_4 for Redwood NP (−0.15 and −0.12). While these values in and of themselves are relatively small, these were the highest at this site that also had *p*-values $< \alpha$. BC contributes to the highest statistically significant negative correlations in five out of seven sites at the two most southerly coastal sites, and at each of the mountainous sites (−0.11, −0.18, −0.12, −0.11, and −0.14). SO_4 amounts are also slightly higher at the southerly mountainous sites and Pinnacles NM (−0.09, −0.12, and −0.08). In terms of 2017 data, Asian dust and SO_4 are the most likely contributors to precipitation suppression at Redwood NP with values of −0.44 and −0.43, respectively. At Point Reyes NS, BC and SO_4 have the highest negative correlations (−0.30 and −0.27). Pinnacles NM, Fresno, Lassen Volcanic, and Bliss all had higher negative correlations of locally influenced dust, BC, and SO_4 (Figure 8). This makes sense for the first three sites as they are more inland, or facing inland (Pinnacles, Fresno, Lassen Volcanic) and located near the southern-most half of northern California.

Table 2. Correlation Analysis between aerosols and precipitation at coastal (RDWD, PTREY, PINN), inland (FRES) and mountainous (LAVO, BLISS, KAIS) sites. Highlighted values are correlations (R-values) with *p*-values less than 0.05. The *p*-values between 0.05 and 0.1 is marked as **.

2007–2016 Correlations								
	Dust (Asian)		**Dust (Non-Asian)**		**Black Carbon**		**Sulfate**	
	R-Value	***p*-Value**	**R-Value**	***p*-Value**	**R-Value**	***p*-Value**	**R-Value**	***p*-Value**
RDWD	−0.15	0.00	0.04	0.48	−0.23	5.21	−0.12	0.02
PTREY	−0.07	0.15	−0.07	0.19	−0.11	0.02	−0.02	0.76
PINN	−0.07	0.14	−0.08	0.10 **	−0.18	0.00	−0.08	0.09 **
FRES	−0.03	0.61	−0.01	0.91	0.02	0.76	−0.03	0.54
LAVO	−0.06	0.22	−0.08	0.09 **	−0.12	0.01	−0.08	0.10 **
BLISS	−0.07	0.14	−0.07	0.14	−0.11	0.02	−0.09	0.06 **
KAIS	−0.09	0.06 **	−0.06	0.20	−0.14	0.01	−0.12	0.02
2017 Correlations								
	Dust (Asian)		**Dust (Non-Asian)**		**Black Carbon**		**Sulfate**	
	R-Value	***p*-Value**	**R-Value**	***p*-Value**	**R-Value**	***p*-Value**	**R-Value**	***p*-Value**
RDWD	−0.44	0.00	−0.17	0.47	−0.64	7.38	−0.43	0.01
PTREY	−0.15	0.37	−0.18	0.26	−0.30	0.06 **	−0.27	0.09 **
PINN	−0.08	0.60	−0.33	0.04	−0.44	0.00	−0.37	0.02
FRES	0.25	0.12	−0.46	0.00	−0.39	0.01	−0.39	0.01
LAVO	−0.23	0.15	−0.36	0.02	−0.47	0.00	−0.39	0.01
BLISS	−0.18	0.26	−0.31	0.04	−0.36	0.02	−0.28	0.08 **
KAIS	−0.14	0.38	−0.19	0.24	−0.20	0.23	−0.20	0.23

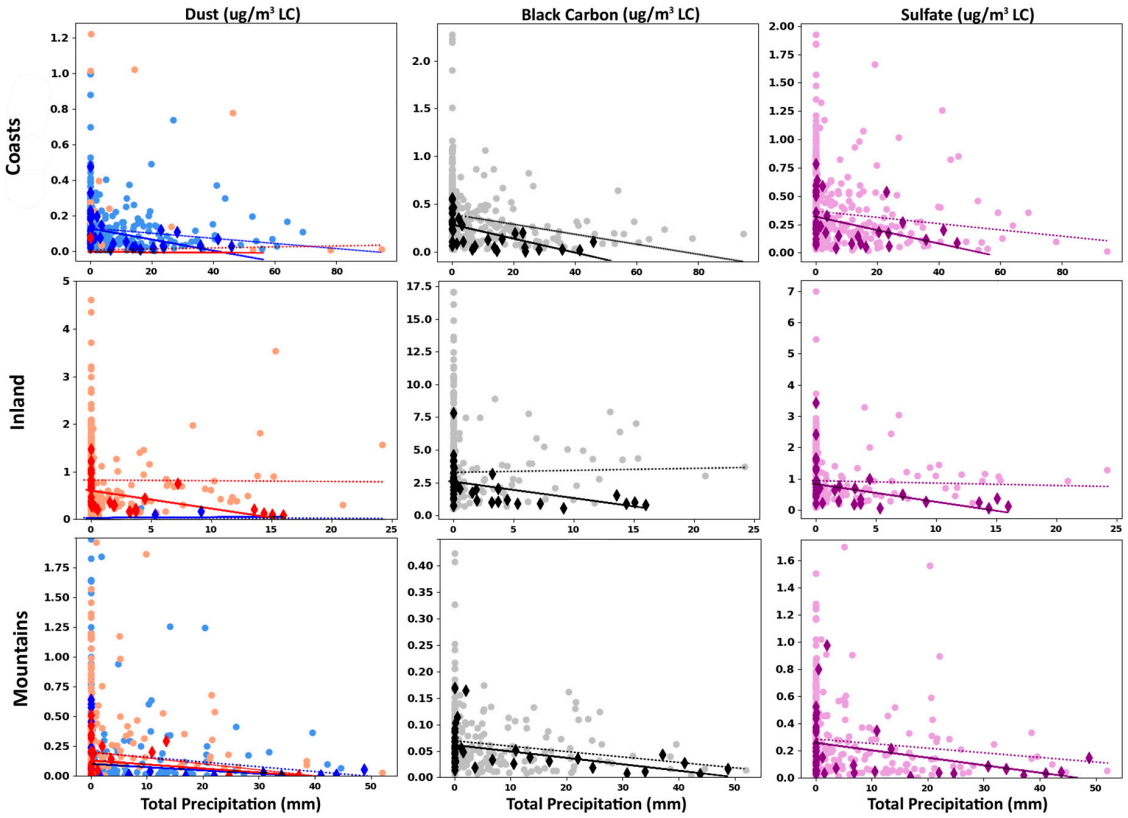

Figure 8. R-value correlations between dust (Asian: Blue, non-Asian: Red), BC, and SO_4 against precipitation. The sites shown are Redwood, Fresno, and Lassen Volcanic to represent coasts, inlands, and mountains, respectively. Climatological data (2007–2016) is represented in the lighter colored circles, while the 2017 data is represented by the darker diamonds.

4.3. HYSPLIT Back Trajectory Analysis

Figure 9a shows the ten-day back trajectories for Redwood NP, Fresno, and Lassen Volcanic NP starting from 01/07 at 23Z. It appears that from each location, air parcels originate from East Asia, in the middle of China, which is most visibly shown from the Lassen Volcanic NP ensemble. Figure 9b shows parcel heights during the back trajectory. Parcels start near the surface, below 900 hPa, for the first few days before being vertically advected to around 450–300 hPa between 01/02 and 01/03. After two to three days, parcels lower to around 700 hPa when they reach the sites.

The 10-day back trajectories and parcel height comparisons at Redwood NP for the ensuing 2017 AR events on 01/07, 01/19, 02/09, and 02/21 are shown in Figure 10. The trajectories of the 3 AR events, as shown in Figure 10a, align with those in Figure 9a suggesting that their origins are to be located between the coast of northern China and Japan. However, it is interesting to note the differences between tracks for each event. For instance, the ensemble trajectories for 01/07 generally show patterns of shorter and steeper ridges and troughs as the parcel is advected over the north Pacific. 01/19 and 02/09, on the other hand, generally display longer and more zonal ridge/trough movement. In Figure 10b, all four events (01/07, 01/19, 02/09, 02/21) show ensemble trajectories where there is steep lifting from the surface to around 450 hPa, with 01/07 and 02/21 being most noticeable. Events with longer/zonal movement generally resulted in lifting from the surface to around 750 hPa, as seen on 01/19 and 02/09, with some air parcels being an exception.

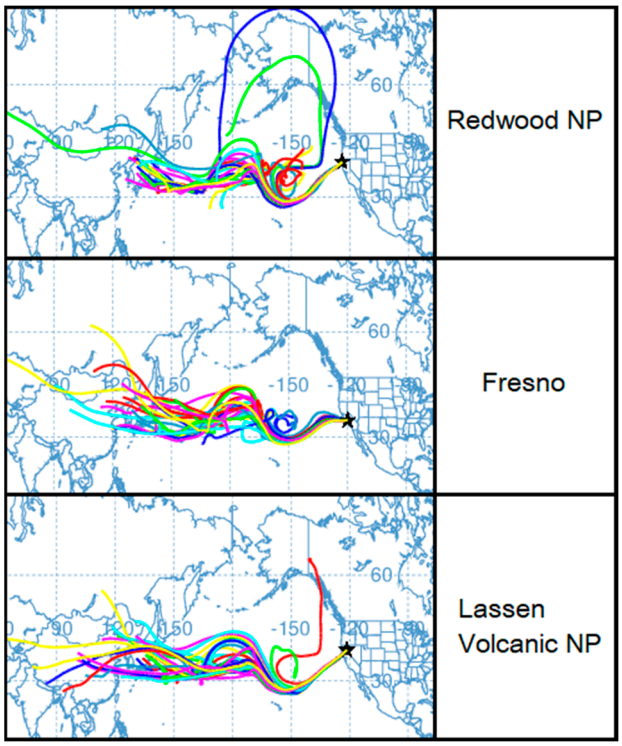

(a)

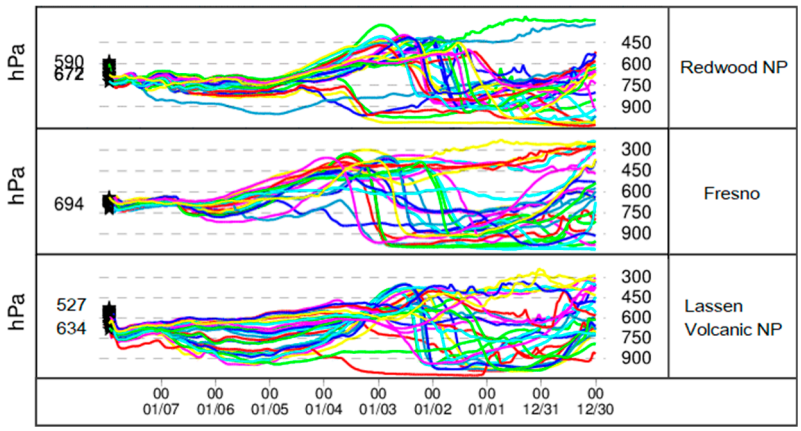

(b)

Figure 9. Hybrid Single-Particle Lagrangian Integrated Trajectory model (HYSPLIT) back trajectories from 01/07. (**a**) Redwood, Fresno, and Lassen Volcanic were shown to represent the coasts, inlands, and mountains, respectively. (**b**) air parcel height levels during the 10-day back trajectories.

This difference could be a possible explanation for the differences in parcel vertical advection as seen in Figure 10b. In general, the majority of parcels are lifted from the surface to higher levels before settling back to the surface. These track patterns follow and agree with the synoptic conditions described in Figure 2.

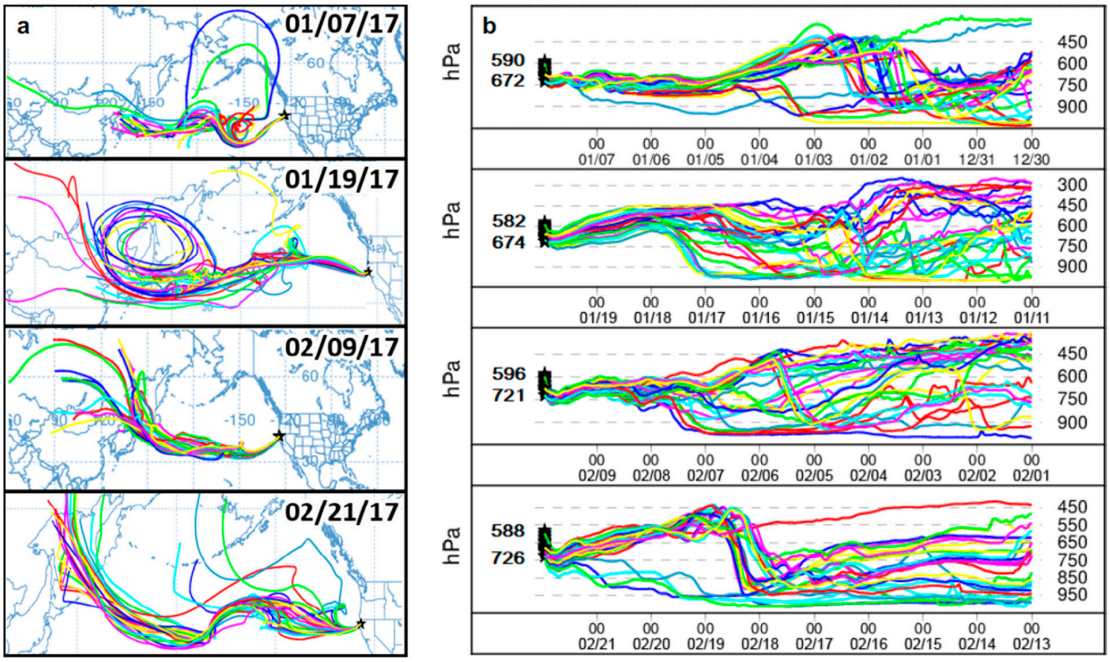

Figure 10. HYSPLIT back trajectories at Redwood NP for (**a**) back trajectories calculated at the first day of 2017 AR events. (**b**) 10-day back trajectories (day 0 to day −9, from left to right) at different heights (hPa).

5. Discussion and Conclusions

Comparing the properties of a 2006–2016 long-term analyses to selected 2017 AR events, the study aimed to understand three main points: (1) The effects of long-range aerosol transport on different terrain regions over Northern California, (2) how aerosols affect precipitation intensity, location, and frequency using IVT as a proxy, and (3) assess how aerosols are correlated with AR- associated precipitation. It is shown that more Asian dust tends to be observed over the coast while more locally produced dust tends to be observed inland. The hypothesis was that aerosols would have enhanced the precipitation from the 2017 AR events (positive correlations). However, based on analysis, dust appears to have a slight suppression of precipitation, particularly farther south in the mountains. Black carbon (BC), on the other hand, shows a slight enhancement of precipitation for sites at higher latitudes than Bliss SP and Kaiser, and closer to the coast, as seen at Pinnacles NP. Sulfate (SO_4) also tended to have slight precipitation suppression. In this study our correlation analysis suggests that the long-range transport of aerosols from East Asia had little evidence of effect on either AR events climatologically or in 2017. Reasons for low R-values could be due to wet deposition and scavenging as aerosols travel across the North Pacific. Locally influenced dust, on the other hand, have statistically significant negative correlations with the precipitation during AR events for the majority of the sites. BC and SO_4 tend to be associated with precipitation suppression, but whether they are transported or locally generated is not clear and this needs to be investigated further in the future study.

In terms of future work, AR events occurring in March–April, where more dust is present, will be compared to AR events occurring in January–February. Also, in part 2 of the study, numerical simulations will also be utilized to compare to observation data collected and model aerosol transport effects on local precipitation and cloud microphysics.

Author Contributions: Writing—Original Draft Preparation, C.L.; writing—Review and Editing, C.L., S.C. and J.R.; Supervision, S.C.

Acknowledgments: We acknowledge the supplies of datasets utilized in this research. SSM/I and SSMIS data are available at www.rmss.com/missions/ssmi. Monthly precipitation visualizations used in this study were produced by Advanced Hydrologic Prediction Service maintained by NOAA's National Weather Service. We also acknowledge the MODIS mission scientists and associated NASA personnel for the production of the data used in

this research. Comments and suggestions by two anonymous reviewers were much appreciated. This research was supported by the NOAA/EPP Cooperative Agreement #NA16SEC4810006, and NASA MUREP-NNX15AQ02A.

Conflicts of Interest: The authors declare no conflict of interest.

References

1. Governor's Drought Declaration. Available online: http://www.water.ca.gov/waterconditions/declaration.cfm (accessed on 30 April 2017).
2. Climate Station Predition Summary. Available online: http://www.cnrfc.noaa.gov/awipsProducts/RNOWRKCLI.php (accessed on 27 April 2017).
3. Dettinger, M. Climate Change, Atmospheric Rivers, and Floods in California—A Multimodel Analysis of Storm Frequency and Magnitude Changes. *JAWRA J. Am. Water Resour. Assoc.* **2011**, *47*, 514–523. [CrossRef]
4. Eiserloh, A.J.; Chiao, S. Modeling studies of landfalling atmospheric rivers and orographic precipitation over northern California. *Meteorol. Atmos. Phys.* **2015**, *127*, 1–16. [CrossRef]
5. Neiman, P.J.; Ralph, F.M.; Wick, G.A.; Lundquist, J.D.; Dettinger, M.D. Meteorological Characteristics and Overland Precipitation Impacts of Atmospheric Rivers Affecting the West Coast of North America Based on Eight Years of SSM/I Satellite Observations. *J. Hydrometeorol.* **2008**, *9*, 22–47. [CrossRef]
6. Ralph, F.M.; Prather, K.A. Calwater Field Studies Designed to Quantify the Roles of Atmospheric River and Aerosols in Modulating U.S. West Coast Precipitation in a Changing Climate. *Am. Meteorol. Soc.* **2016**, 1209–1228. [CrossRef]
7. Rutz, J.J.; Steenburgh, W.J.; Ralph, F.M. Climatological Characteristics of Atmospheric Rivers and Their Inland Penetration over the Western United States. *Mon. Weather Rev.* **2014**, *142*, 905–921. [CrossRef]
8. Wang, Y.; Wang, M.; Zhang, R.; Ghan, S.J.; Lin, Y.; Hu, J.; Pan, B.; Levy, M.; Jiang, J.H.; Molina, M.J.; et al. Assessing the effects of anthropogenic aerosols on Pacific storm track using a multiscale global climate model. *Proc. Natl. Acad. Sci. USA* **2014**, *111*, 6894–6899. [CrossRef] [PubMed]
9. Ding, A.; Wang, T.; Fu, C. Transport characteristics and origins of carbon monoxide and ozone in Hong Kong, South China. *J. Geophys. Res. Atmos.* **2013**, *118*, 9475–9488. [CrossRef]
10. Creamean, J.M.; Suski, K.J.; Rosenfeld, D.; Cazorla, A.; DeMott, P.J.; Sullivan, R.C.; White, A.B.; Ralph, F.M.; Minnis, P.; Comstock, J.M.; et al. Dust and Biological Aerosols from the Sahara and Asia Influence Precipitation in the Western U.S. *Science* **2013**, *339*, 1572–1578. [CrossRef]
11. Liang, Q.; Jaeglé, L.; Jaffe, D.A.; Weiss-Penzias, P.; Heckman, A.; Snow, J.A. Long-range transport of Asian pollution to the northeast Pacific: Seasonal variations and transport pathways of carbon monoxide. *J. Geophys. Res. Atmos.* **2004**, *109*. [CrossRef]
12. Wang, K.; Zhang, Y.; Jang, C.; Phillips, S.; Wang, B. Modeling intercontinental air pollution transport over the trans-pacific region in 2001 using the community multiscale air quality modeling system. *J. Geophys. Res. Atmos.* **2009**, *114*, 1–23. [CrossRef]
13. Zhang, R.; Li, G.; Fan, J.; Wu, D.L.; Molina, M.J. Intensification of Pacific storm track linked to Asian pollution. *Proc. Natl. Acad. Sci. USA* **2007**, *104*, 5295–5299. [CrossRef] [PubMed]
14. Creamean, J.M.; Axson, J.L.; Bondy, A.L.; Craig, R.L.; May, N.W.; Shen, H.; Weber, M.H.; Pratt, K.A.; Ault, A.P. Atmospheres and elevation in the California Sierra Nevada. *J. Geophys. Res. Atmos.* **2016**, 7296–7309. [CrossRef]
15. Fan, J.; Fan, J.; Leung, L.R.; DeMott, P.J.; Comstock, J.M.; Singh, B.; Rosenfeld, D.; Tomlinson, J.M.; White, A.; Prather, K.A.; et al. Aerosol impacts on California winter clouds and precipitation during calwater 2011: Local pollution versus long-range transported dust. *Atmos. Chem. Phys.* **2014**, *14*, 81–101. [CrossRef]
16. Ault, A.P.; Williams, C.R.; White, A.B.; Neiman, P.J.; Creamean, J.M.; Gaston, C.J.; Ralph, F.M.; Prather, K.A. Detection of Asian dust in California orographic precipitation. *J. Geophys. Res. Atmos.* **2011**, *116*, 1–15. [CrossRef]
17. Patil, N.; Dave, P.; Venkataraman, C.; Crawford, I.; Rasch, P.J. Contrasting influences of aerosols on cloud properties during deficient and abundant monsoon years. *Sci. Rep.* **2017**, *7*. [CrossRef] [PubMed]
18. Heald, C.L.; Jacob, D.J.; Park, R.J.; Alexander, B.; Fairlie, T.D.; Yantosca, R.M.; Chu, D.A. Transpacific transport of Asian anthropogenic aerosols and its impact on surface air quality in the United States. *J. Geophys. Res. Atmos.* **2006**, *111*, 1–13. [CrossRef]

19. National Weather Service: AHPS Precipitation Analysis 2018. Available online: https://water.weather.gov/precip/index.php?location_type=wfo&location_name=mtr (accessed on 31 December 2018).
20. Santa Clara Valley Water District, 2017: 2017 Flooding REPORT FINAL. Available online: https://www.valleywater.org/sites/default/files/2017FloodReport.pdf (accessed on 31 December 2018).
21. Center for Western Weather and Water Extremes, 2017: CW3E AR Update. Available online: http://cw3e.ucsd.edu/author/cw3e-web/page/12/ (accessed on 31 December 2018).
22. White, A.B.; Moore, B.J.; Gottas, D.J.; Neiman, P.J. Winter Storm Conditions Leading to Excessive Runoff above California's Oroville Dam during January and February 2017. *Bull. Am. Meteorol. Soc.* **2018**. [CrossRef]
23. Thorncroft, C.D.; Hoskins, B.J.; McIntyre, M.E. Two paradigms of baroclinic-wave life-cycle behaviour. *Q. J. R. Meteorol. Soc.* **1993**, *119*, 17–55. [CrossRef]
24. Wentz, F.J.; Hilburn, K.A.; Smith, D.K. *Remote Sensing Systems DMSP SSMIS Daily Environmental Suite on 0.25 Deg Grid*; Version 7; Northern Pacific; Remote Sensing Systems: Santa Rosa, CA, USA, 2012; Available online: http://www.remss.com/missions/ssmi (accessed on 13 August 2017).
25. Interagency Monitoring Protected Visual Environment (IMPROVE) Program. Available online: http://vista.cira.colostate.edu/Improve/improve-program/ (accessed on 6 June 2017).
26. Creamean, J.M.; Lee, C.; Hill, T.C.; Ault, A.P.; DeMott, P.J.; White, A.B.; Ralph, F.M.; Prather, K.A. Chemical properties of insoluble precipitation residue particles. *J. Aerosol Sci.* **2014**, *76*, 13–27. [CrossRef]
27. VanCuren, R.A.; Cliff, S.S.; Perry, K.D.; Jimenez-Cruz, M. Asian continental aerosol persistence above the marine boundary layer over the eastern North Pacific: Continuous aerosol measurements from Intercontinental Transport and Chemical Transformation 2002 (ITCT 2 K2). *J. Geophys. Res.* **2005**, *110*. [CrossRef]
28. Ralph, F.M.; Rutz, J.J.; Cordeira, J.M.; Dettinger, M.; Anderson, M.; Reynolds, D.; Schick, L.J.; Smallcomb, C. A Scale to Characterize the Strength and Impacts of Atmospheric Rivers. *Bull. Am. Meteor. Soc.* **2019**. [CrossRef]